Preprint, for final version see Journal of Applied Mechanics 81(3), 034505 (Oct 16 2013) http://dx.doi.org/10.1115/1.402527013.

A Simple Model for Axial Displacement in a Cylindrical Pipe with Internal Shock Loading

Neal P. Bitter and Joseph E. Shepherd

Graduate Aerospace Laboratories

California Institute of Technology

Pasadena, California 91125

Email: nbitter@caltech.edu

ABSTRACT

This paper describes a simplified model for predicting the axial displacement, stress, and strain in pipes subjected to internal shock waves. This model involves the neglect of radial and rotary inertia of the pipe, so its predictions represent the spatially-averaged or low-pass filtered response of the tube. The simplified model is developed first by application of the physical principles of conservation of mass and momentum on each side of the shock wave. This model is then reproduced using the mathematical theory of the Green's function, which allows other load and boundary conditions to be more easily incorporated. Comparisons with finite element simulations demonstrate that the simple model adequately captures the tube's axial motion except near the critical velocity corresponding to the bar wave speed $\sqrt{E/\rho}$. Near this point the simplified model, despite being an unsteady model, predicts a time-independent resonance while the finite element model predicts resonance that grows with time.

Introduction

Extensive experimental observations of the structural response of pipes and tubes to internal shock and detonation wave loading have been carried out over the last decade at the Explosion Dynamics Laboratory, as documented in [1,2]. These observations consist primarily of point measurements of strain which have been extremely useful for quantitative characterization of structural loading as well as point validation of simulations. However, due to the large number of potential vibration modes and the stiffness of typical piping systems, it is often difficult to infer the global response due to the confounding presence of high-frequency oscillations in strain signals. Finite-element simulations and reduced order models are particularly useful tools to use in conjunction with experiments to gain insight into large-scale, lower frequency, response modes. This note presents an analysis of the axial displacement induced by shock loading and proposes a simplified but quantitatively predictive model.

Numerical Simulation Results

One example for which we have carried out an analysis is a finite-element simulation (LS-Dyna) of a shock wave with a pressure rise of 2.52 MPa traveling at 2088 m/s in 2-m long section of 2-in diameter schedule 40 stainless steel pipe (see Table 1). This example is relevant to the evaluation of the structural response of piping in the Hydrogen in Pipes and Ancillary Vessels (HPAV) evaluation carried out for the Waste Treatment Plant at the Hanford Site [3,4].

Typical results are shown in Figs. 1 and 2 for at a time of 225 μs, before any wave reflections occur from the RHS end of the pipe. The shock wave propagates with constant speed, starting from the origin at the LHS and propagating toward the right. The fluid dynamics associated with the shock wave are not considered as we are only interested in the structural response of the pipe to an idealized traveling load. The boundary conditions are zero axial and radial displacement at each end of the pipe. The pipe is modeled as a linear elastic solid with Young's modulus $E = 1.93 \times 10^{11}$ Pa, density $\rho = 8040$ kg/m^3, and Poisson's ratio $\nu = 0.30$. The inner radius of the pipe is 26.25 mm and the wall thickness is 3.91 mm. For the membrane model of motion discussed subsequently, the effective membrane radius $a = 28.2$ mm and the ratio $a/h = 7.2$.

The radial displacement w and axial displacement u propagate as progressive wave systems as shown in Fig. 3.

The leading edge of the wave is moving at approximately the bar wave speed $\upsilon_b = \sqrt{E/\rho} = 4900$ m/s and the waveform is an approximately bilinear displacement field $u(x,t)$ with a maximum amplitude u_p moving at the speed of the shock wave front υ. The entire structure is self-similar if the shock speed is constant and pressure is uniform behind the shock. The maximum amplitude of the displacement increases in magnitude approximately linearly in time $u_p = \dot{u}_p t$, where $\dot{u}_p < 0$. Small oscillations in axial displacement are superposed on the main bilinear profile. These are primarily a consequence of the large oscillations in radial displacement shown in Fig. 1 and the Poisson coupling between radial and axial strain. Additional contributions are due to the excitation of shear waves in the region just ahead of the shock front and propagation of axial disturbances ahead of the front created by the periodic motion behind the front.

The radial displacement w and hoop strain $\varepsilon_\theta = w/a$ show very substantial oscillations behind the shock front and much smaller oscillations ahead. The response behind the shock front is periodic in space and also in time, with an oscillation frequency of approximately

$$f_h = \frac{1}{2\pi a}\sqrt{\frac{E}{\rho(1-\nu^2)}} \tag{1}$$

and a spatial wavelength of $\lambda_h = \upsilon/f_h$. The oscillatory motion is determined by the tube inertia and the symmetric radial motion being opposed primarily by the hoop stress associated with radial displacement as discussed in [5]. Numerically, this frequency is 29 kHz and the associated spatial wavelength behind the front is 72 mm. The axial displacement oscillations are much more apparent in axial strain (Fig. 2) due to the amplifying effects of differentiation used to obtain strain from displacement, $\varepsilon_x = \partial u/\partial x$. The evolution of the axial displacement wave with time can be more clearly visualized if the profiles at different times are overlaid, shown in Fig. 4. This method of presentation shows that for the case of zero displacement at the pipe LHS, the displacement field to the left of the pressure wave front is in steady state.

Membrane Model

Motivated by the simple form of the axial displacement waves shown in Fig. 3, we seek a model of the axial displacement that focuses on axial wave motion and simplifies or eliminates the high-frequency oscillations that

are prominent in the axial strain results. The first step is to approximate the pipe as a shell without any shear deformation or rotary inertia. This will eliminate the high frequency oscillations observed in the axial strain just ahead of the pressure front in Fig. 2. The second step is to consider the shell as a membrane without any bending stiffness or radial inertia to eliminate radial displacement oscillations, i.e., the radial motion is quasi-steady in character. This will eliminate the hoop mode oscillations observed in the radial displacement but will create discontinuities in radial displacement at the shock front as well as at the shell endpoints. Including bending stiffness would smear these discontinuities over the characteristic bending length of the shell so this needs to be kept in mind when interpreting the model results.

In adopting a quasi-steady membrane model of radial motion, we are effectively time-averaging the radial displacement oscillations behind the front, replacing these by a mean response. This is a reasonable approximation as long as the time scales of the radial oscillation are much smaller than the axial wave propagation times. In the example discussed above, the period of radial oscillation is 34 μs and the time for pressure wave to travel the length of the pipe (2 m) is 958 μs. So approximately 28 hoop oscillation cycles will occur in the time it take the pressure wave to traverse the length of the pipe.

The axial motion of the tube is modeled using the following axial force balance:

$$\rho h \frac{\partial^2 u}{\partial t^2} = \frac{\partial N_x}{\partial x} \tag{2}$$

where N_x is the axial stress resultant, defined as the integral of axial stress through the wall thickness. Since we are neglecting the radial dynamics and axial bending of the pipe and balancing the hoop stress against the pressure load, the Lamé solution [6] for a thick-walled pressure vessel can be used to model the variation of hoop and radial stresses through the wall thickness. This model is valid only in regions of the pipe where the axial strain is uniform in both the axial and radial directions, but due to our neglect of axial bending and rotary inertia these conditions are met everywhere except near the load front and the boundaries of the pipe. As a result, the use of the Lamé solution is consistent with the assumptions already made in developing this simplified model. Note that for thin tubes, one can alternatively use the thin shell approximations $\sigma_r << \sigma_\theta$ and $\sigma_\theta = Pa/h$, but in the present formulation the thick-wall effects can be included without additional difficulty.

The Lamé solutions for the hoop and radial stresses in a long cylinder are the following:

$$\sigma_\theta(r) = \frac{PR_i^2}{R_i^2 - R_o^2}\left(1 + \frac{R_o^2}{r^2}\right) \tag{3a}$$

$$\sigma_r(r) = \frac{PR_i^2}{R_i^2 - R_o^2}\left(1 - \frac{R_o^2}{r^2}\right) \tag{3b}$$

where R_i and R_o are the inner and outer radii of the tube. From Hooke's law, the axial stress is then:

$$\begin{aligned}\sigma_x &= E\varepsilon_x + \nu(\sigma_r + \sigma_\theta) \\ &= E\varepsilon_x + \nu\frac{2PR_i^2}{R_o^2 - R_i^2}\end{aligned} \tag{4}$$

The axial stress resultant N_x is found by integrating σ_x through the wall thickness. Since in this case σ_x is uniform through the thickness, the result is:

$$N_x = Eh\varepsilon_x + \nu\frac{2PhR_i^2}{R_o^2 - R_i^2} \tag{5}$$

It may be noted that the wall thickness is $h = R_o - R_i$ and the mean radius is $a = 0.5(R_o + R_i)$. Using these definitions, the axial stress resultant can be expressed in the form:

$$N_x = Eh\varepsilon_x + \nu Pa\left(\frac{R_i^2}{a^2}\right) \tag{6}$$

The quantity in parenthesis is the correction due to thick-wall effects, which will hereafter be denoted C_t. As the wall thickness is reduced, this factor approaches 1.0 and the expression that remains is the result from classical thin shell theory. In this paper, the correction term must be retained since we are analyzing a tube with inner radius $R_i = 26.25$ mm and mean radius $a = 28.2$ mm, which gives a correction factor of $C_t = 0.866$.

Upon inserting (6) into (2) and replacing $\varepsilon_x = \partial u/\partial x$ we obtain:

$$\frac{1}{\upsilon_b^2}\frac{\partial^2 u}{\partial t^2} - \frac{\partial^2 u}{\partial x^2} = C_t\frac{\nu a}{Eh}\frac{\partial P}{\partial x} \tag{7}$$

where υ_b is the bar wave speed $\sqrt{E/\rho}$. This result is a wave equation for the axial displacement u which is forced by the gradient of pressure. For a thin tube, the correction factor C_t tends to 1.0 and the quantity $\nu Pa/Eh$ is the

quasi-static radial displacement of the tube from classical thin shell theory. Thus the forcing term can also be interpreted as the gradient of the quasi-static radial displacement.

In the context of traveling shock waves, the pressure distribution is modeled as:

$$P(x,t) = P_o \Theta(\upsilon t - x) \tag{8}$$

where Θ is the Heaviside step function and υ is the speed of the shock wave. Under this load, (7) becomes:

$$\frac{1}{\upsilon_b^2}\frac{\partial^2 u}{\partial t^2} - \frac{\partial^2 u}{\partial x^2} = C_t \frac{\nu P_o a}{Eh}\delta(\upsilon t - x) \tag{9}$$

where $\delta(x)$ is the Dirac delta function. In this case, the source term vanishes everywhere except at the shock front $x = \upsilon t$ and the axial wave motion of the tube is driven solely by the discontinuity in pressure (which results in a jump in hoop, axial, and radial stresses) at the wavefront.

Observations on the Numerical Simulation Results

The numerical solution exhibits a linear growth in time for both the spatial extent and amplitude of the axial displacement u. The point of maximum displacement amplitude u_p moves with the speed of the pressure wave and as shown in Fig. 5, and grows linearly with time with a speed of $\dot{u}_p$ = -0.035 m/s.

The axial displacement also shows a nearly linear variation with distance (Fig. 4) in the segments of the wave ahead and behind the pressure wave front. We will therefore idealize the strain in these segments as time-independent with distinct values ahead $\varepsilon_{x,1}$ and behind $\varepsilon_{x,2}$ of the wave front. From the continuity of the axial displacement at the pressure wave front, we can integrate the strain through the wave to relate the two strain magnitudes to the wave speeds and obtain the following relationship:

$$\varepsilon_{x,1} = -\frac{\upsilon}{\upsilon_b - \upsilon}\varepsilon_{x,2} \tag{10}$$

In terms of $\dot{u}_p$, the idealized strains can computed to be

$$\varepsilon_{x,1} = -\frac{\dot{u}_p}{\upsilon_b - \upsilon} \tag{11}$$

and

$$\varepsilon_{x,2} = \frac{\dot{u}_p}{\upsilon} \tag{12}$$

Solution of the Model Equations

Based on the results of the numerical simulations, we can divide the solution domain into three segments:

Region 0: $\upsilon_b t \leq x \leq L$. Ahead of bar wave front there is no disturbance and the axial displacement vanishes. Once the wave reaches the RHS of the pipe, $x = L$, a reflected wave propagating the left is created in order to satisfy the boundary condition. This wave can be readily computed using the method of characteristics [7] but in the interest of brevity, will not be considered in this note. With this limitation, the solution is simply

$$u(x,t) = 0 \qquad \text{for} \qquad \upsilon_b t \leq x \leq L \tag{13}$$

Region 1: $\upsilon t \leq x \leq \upsilon_b t$ Between the pressure wave front and the bar wave front, the axial displacement propagates as a right facing wave with constant axial strain $\varepsilon_{x,1}$ and stress resultant $N_{x,1}$. The magnitude of the strain was given above by (11). Since the pressure is zero in this region, the axial stress resultant (6) reduces to

$$N_x = Eh\varepsilon_x \tag{14}$$

which is consistent with the state of uni-axial strain ahead of the pressure wave front. From the theory of characteristics for wave equations [7], the axial displacement in this region has the general form

$$u = f(x - \upsilon_b t) \tag{15}$$

From the assumption of constant axial strain in this region we conclude that

$$u(x,t) = \varepsilon_{x,1}\left(x - \upsilon_b t\right) \tag{16}$$

which consistent with our previous observations. This implies that

$$\frac{\partial u}{\partial t} = -\varepsilon_{x,1}\upsilon_b \tag{17}$$

$$\frac{\partial u}{\partial x} = \varepsilon_{x,1} \tag{18}$$

Using (11), we can write the displacement field as

$$u(x,t) = -\frac{\dot{u}_p}{\upsilon_b - \upsilon}\left(x - \upsilon_b t\right) \qquad \text{for} \qquad \upsilon t \leq x \leq \upsilon_b t \tag{19}$$

Region 2: $0 \leq x \leq \upsilon t$ - Between the LHS ($x = 0$) of the pipe and the pressure wave front $x = \upsilon t$, the displacement is steady (independent of time) and linearly proportional to the distance from the LHS of the pipe.

$$\frac{\partial u}{\partial t} = 0 \tag{20}$$

$$\frac{\partial u}{\partial x} = \varepsilon_{x,2} \tag{21}$$

This can be integrated to yield the complete solution

$$u(x,t) = \varepsilon_{x,2} x \tag{22}$$

The axial stress resultant in this region is

$$N_{x,2} = Eh\varepsilon_{x,2} + \nu aPC_t \tag{23}$$

Using (12), we can write the displacement field as

$$u(x,t) = \frac{\dot{u}_p}{\upsilon} x \qquad \text{for} \qquad 0 \le x \le \upsilon t \tag{24}$$

In order to complete the solution, we need one more relationship to determine the value of the strain in either region 1 or 2 or else the magnitude of $\dot{u}_p$. An additional relationship can be obtained by considering the axial force balance in the shell on each side of the pressure front. In general, the axial stress resultants on each side will be different in order to have a balance of momentum at the front that correctly accounts for the jump in material velocity $V = \partial u/\partial t$ through the front.

The simplest way to construct the balance of momentum is to consider a fixed control volume that encloses the shell. At time t the left boundary of the control volume is in region 2 just behind the pressure front, and the right boundary is well in front of the bar wave, completely enclosing region 1. Recognizing that the velocity in region 2 is zero, the change in momentum in a time Δt will be the sum of the loss of momentum in the shell material that is brought to rest by the motion of the front and the gain of momentum due to the motion of the bar wave. This has to be balanced by the impulse applied to the control volume by the stress resultant in region 2, since the stress resultant ahead of region 1 vanishes. The resulting momentum balance is

$$-N_{x,2}\Delta t = \rho h \left(\upsilon_b - \upsilon\right) V_1 \Delta t \tag{25}$$

Substituting for the axial stress resultant and the velocity, we have

$$Eh\varepsilon_{x,2} + \nu a P C_t = -\rho h \left(\upsilon_b - \upsilon\right)\left(-\varepsilon_{x,1}\upsilon_b\right) \tag{26}$$

Substitutions of expressions for axial strains (11) and (12) leads to

$$\dot{u}_p = -\nu \frac{\upsilon\upsilon_b}{\upsilon_b + \upsilon} \frac{a}{h} \frac{P}{E} C_t \tag{27}$$

$$\varepsilon_{x,2} = -\nu \frac{\upsilon_b}{\upsilon_b + \upsilon} \frac{a}{h} \frac{P}{E} C_t \tag{28}$$

$$\varepsilon_{x,1} = +\nu \frac{\upsilon\upsilon_b}{\upsilon_b^2 - \upsilon^2} \frac{a}{h} \frac{P}{E} C_t \tag{29}$$

From Hooke's law, the hoop strain is given by:

$$\varepsilon_\theta = \frac{1}{E}\left[\sigma_\theta - \nu(\sigma_x + \sigma_r)\right] \tag{30}$$

At the outer surface of the tube, σ_r is zero and in region 2, σ_θ and σ_x are evaluated using (3a) and (4). Using these equations, the hoop strain at the outer surface in region 2 is found to be:

$$\varepsilon_{\theta,2} = \left(1 - \nu^2 \frac{\upsilon}{\upsilon_b + \upsilon}\right) \frac{Pa}{Eh} C_t \tag{31}$$

In region 1, both σ_r and σ_θ are zero, so the application of (30) gives:

$$\varepsilon_{\theta,1} = -\nu^2 \frac{\upsilon \upsilon_b}{\upsilon_b^2 - \upsilon^2} \frac{Pa}{Eh} C_t \tag{32}$$

As expected, $\varepsilon_{\theta,2}$ is intermediate between the limiting cases of zero axial strain, $\varepsilon_{x,2} = 0$, and zero axial stress, $N_{x,2} = 0$, which give the limits

$$\left(1 - \nu^2\right) \frac{Pa}{Eh} C_t \le \varepsilon_{\theta,2} \le \frac{Pa}{Eh} C_t \tag{33}$$

Substituting the parameters listed in Table 1, we obtain the numerical values given in Table 2. The corresponding LS-Dyna simulation results were analyzed to extract mean values for comparison to the model. Given the simplifications of the model, the results compare favorably with the values computed by the transient finite-element solution.

Green's Function Solution

The exact solution for the axial displacements can also be found using the mathematical technique of the Green's function. To do so, (7) will be solved on a semi-infinite interval $[0,\infty]$ with the boundary condition $u(0,t) = 0$ at the origin. The Green's function $g(x,x_o,t,t_o)$ is found by replacing the inhomogeneous term in (7) by spatial and temporal Dirac delta functions:

$$\frac{1}{\upsilon_b^2}\frac{\partial^2 g}{\partial t^2} - \frac{\partial^2 g}{\partial x^2} = \delta(x - x_o)\delta(t - t_o) \tag{34}$$

The Green's function satisfying this equation is given by [8]:

$$\begin{aligned} g(x,x_o,t,t_o) &= \frac{\upsilon_b}{2}\Theta\Big(\upsilon_b(t-t_o)-|x-x_o|\Big) \\ &= \begin{cases} \frac{\upsilon_b}{2} & |x-x_o|<\upsilon_b(t-t_o) \\ 0 & |x-x_o|>\upsilon_b(t-t_o) \end{cases} \end{aligned} \tag{35}$$

where Θ is the Heaviside function. Solutions to the inhomogeneous wave equation (7) are found by integrating the Green's function against the source term:

$$u(x,t) = \int_0^t \int_{-\infty}^{\infty} g(x,x_o,t,t_o) C_t \frac{\nu a}{Eh} \frac{\partial}{\partial x_o} P(x_o,t_o) dx_o dt_o \tag{36}$$

We are only interested in solutions on the interval $[0,\infty]$, but in order to evaluate this integral it is necessary to specify the pressure $P(x_o,t_o)$ for $x_o<0$. To satisfy the boundary condition $u(0,t)=0$, the pressure distribution is mirrored symmetrically about the origin, i.e.,

$$P(-x_o,t_o) = P(x_o,t_o) \tag{37}$$

Since the Green's function is only non-zero when $|x-x_o|<\upsilon_b(t-t_o)$, the limits of the spatial integral in (36) are replaced by finite values and the solution can be written as

$$u(x,t) = C_t \frac{\upsilon_b}{2} \frac{\nu a}{Eh} \int_0^t \int_{x-\upsilon_b(t-t_o)}^{x+\upsilon_b(t-t_o)} \frac{\partial}{\partial x_o} P(x_o,t_o) dx_o dt_o \tag{38}$$

which is readily integrated to obtain:

$$\begin{aligned} u(x,t) = C_t \frac{\upsilon_b}{2} \frac{\nu a}{Eh} \int_0^t & P\Big(x+\upsilon_b(t-t_o),t_o\Big) \\ & - P\Big(x-\upsilon_b(t-t_o),t_o\Big) dt_o \end{aligned} \tag{39}$$

The above result is valid for an arbitrary pressure distribution. We now specialize to the case of a shock wave traveling at velocity υ, for which the pressure is a step function of amplitude P_o:

$$P(x_o,t_o) = P_o\Theta(\upsilon t_o - x_o) \tag{40}$$

Equation (39) can be interpreted as the integral of the applied pressure P along the C^+ and C^- characteristics, where integration along these paths is parameterized by t_o. This situation is shown schematically on an x-t diagram in Fig. 6. The right half of the diagram depicts the domain of interest, while the left half is the mirror image used to satisfy the zero displacement boundary condition. There are two waves in the region of interest. The faster wave, traveling at a speed $\mathfrak{v}_b$, is the leading characteristic and in front of this wave (Region 0) no motion of the tube occurs. The slower wave, traveling at speed $\mathfrak{v}$, is the applied pressure load. Within the shaded region on this plot, the applied pressure is constant and equal to P_o, while outside this region the pressure is zero.

In this diagram we are seeking the solution u at a pair of coordinates (x,t). As represented in (39), the solution at this point is found by integrating the pressure along the C^+ and C^- characteristics, shown as dashed lines in the figure. If the point of interest lies in Region 2, as depicted by point (x_a,t_a), then both the C^+ and C^- characteristics pass through the shaded region where the pressure is nonzero. On the other hand, for a point such as (x_b,t_b) lying in Region 1, only the C^+ characteristic passes through the shaded region. As a result, the form of the solution is different in each of these regions.

Region 2

To evaluate (39) in Region 2, we need only to integrate from $t_1 < t_o < t$ along the C^+ characteristic and from $t_2 < t_o < t$ along the C^- characteristic, where t_1 and t_2 are the times at which the characteristics intersect the pressure wavefront. Thus (39) becomes:

$$\begin{aligned} u(x,t) &= C_t \frac{\mathfrak{v}_b}{2} \frac{\nu a}{Eh} \left[\int_{t_1}^{t} P_o dt_o - \int_{t_2}^{t} P_o dt_o \right] \\ &= C_t \frac{\mathfrak{v}_b}{2} \frac{\nu a}{Eh} P_o (t_1 - t_2) \end{aligned} \tag{41}$$

From the geometry of the problem, the times t_1 and t_2 are found to be:

$$t_1 = \frac{\mathfrak{v}_b t - x}{\mathfrak{v} + \mathfrak{v}_b} \tag{42a}$$

$$t_2 = \frac{x + \mathfrak{v}_b t}{\mathfrak{v} + \mathfrak{v}_b} \tag{42b}$$

Thus the displacement in region 2 is given by:

$$u(x,t) = -C_t \frac{\nu a}{Eh} P_o \left(\frac{\upsilon_b}{\upsilon + \upsilon_b} \right) x \qquad (x < \upsilon t) \tag{43}$$

Region 1

The solution in Region 1 is found using the same approach; however, only the C^+ characteristic passes through the shaded region in Fig. 6. As a result, (39) becomes:

$$u(x,t) = C_t \frac{\upsilon_b}{2} \frac{\nu a}{Eh} P_o (t_4 - t_3) \tag{44}$$

Referring to Fig. 6, t_3 is exactly the same as t_1 above and t_4 is given by:

$$t_4 = \frac{x - \upsilon_b t}{\upsilon - \upsilon_b} \tag{45}$$

Hence the displacement in region 1 becomes:

$$u(x,t) = C_t \frac{\nu a}{Eh} P_o \left(\frac{\upsilon \upsilon_b}{\upsilon_b^2 - \upsilon^2} \right) (x - \upsilon_b t) \qquad (x > \upsilon t) \tag{46}$$

A plot comparing the axial displacement predicted by this simple model with finite element simulations (using conditions from Table 1) is shown in Fig. 7. The simplified model captures the axial motion remarkably well given the level of simplification involved.

Strains and Stresses

By differentiating the displacements, the strains are found to be:

$$\varepsilon_x = \begin{cases} -C_t \frac{\nu a}{Eh} P_o \left(\frac{\upsilon_b}{\upsilon + \upsilon_b} \right) & x < \upsilon t \\ +C_t \frac{\nu a}{Eh} P_o \left(\frac{\upsilon \upsilon_b}{\upsilon_b^2 - \upsilon^2} \right) & x > \upsilon t \end{cases} \tag{47}$$

These expressions are exactly the same as those determined in (28-29) using mass and momentum balances. Making use of the definition (6), the axial stress resultant is found to be:

$$\frac{N_x}{P_o a C_t} = \begin{cases} \nu\left(\frac{\upsilon}{\upsilon+\upsilon_b}\right) & x < \upsilon t \\ \nu\left(\frac{\upsilon\upsilon_b}{\upsilon_b^2-\upsilon^2}\right) & x > \upsilon t \end{cases} \tag{48}$$

A similar analysis can be performed for the case of a pressure load that is supersonic relative to the bar wave velocity ($\upsilon > \upsilon_b$), and expressions for the axial displacement u under these conditions are provided in Table 3.

We have also reproduced these results by taking the semi-infinite Fourier sine transform of (7) and solving the resulting temporal ordinary differential equation. Upon inverting the transform, the following form of solution is obtained:

$$u(x,t) = C_t \frac{\nu a}{Eh} P_o \frac{1}{2}\left(\frac{\upsilon_b}{\upsilon_b^2-\upsilon^2}\right)\left[\upsilon\Big(|x+\upsilon_b t| - |x-\upsilon_b t|\Big) - \upsilon_b\Big(|x+\upsilon t| - |x-\upsilon t|\Big)\right] \tag{49}$$

This result is equivalent to (43) and (46), but conveniently encapsulates the displacements for regions 0, 1, and 2 as well as the subsonic ($\upsilon < \upsilon_b$) and supersonic ($\upsilon > \upsilon_b$) cases in a single expression.

Zero-Stress Boundary Conditions

In addition to the boundary condition $u(0,t) = 0$ used in the preceding sections, a second practical boundary condition is one of zero axial stress: $N_x(0,t) = 0$. This could correspond to a pipe with a capped end, such that the end of the pipe is free to translate axially. Referring to (6), this boundary condition is equivalent to:

$$\left.\frac{\partial u}{\partial x}\right|_{x=0} = -\nu\frac{P_o a}{Eh} C_t \tag{50}$$

Since any linear function of x and t satisfies the wave equation (7), it is possible to add such a function $y(x,t)$ to the above solution $u(x,t)$ in order to satisfy zero-stress boundary conditions rather than zero-displacement. The

function which satisfies this property is:

$$y(x,t) = -\nu C_t \frac{Pa}{Eh}\left(\frac{\upsilon}{\upsilon_b+\upsilon}\right)(x-\upsilon_b t) \tag{51}$$

After adding this function to $u(x,t)$ from (43) and (46), the resulting displacement field for conditions of zero axial stress is the following:

$$u(x,t) = -\nu C_t \frac{P_o a}{Eh}\begin{cases} x - \frac{\upsilon\upsilon_b}{\upsilon+\upsilon_b}t & x < \upsilon t \\ -\frac{\upsilon^2}{\upsilon_b^2-\upsilon^2}(x-\upsilon_b)t & x > \upsilon t \end{cases} \tag{52}$$

The corresponding strain is:

$$\varepsilon_x = -\nu C_t \frac{P_o a}{Eh}\begin{cases} 1 & x < \upsilon t \\ -\frac{\upsilon^2}{\upsilon_b^2-\upsilon^2} & x > \upsilon t \end{cases} \tag{53}$$

And the axial stress resultant is:

$$\frac{N_x}{P_o a C_t} = \begin{cases} 0 & x < \upsilon t \\ \nu\frac{\upsilon^2}{\upsilon_b^2-\upsilon^2} & x > \upsilon t \end{cases} \tag{54}$$

Once again, similar expressions can be obtained for the case of a supersonic load ($\upsilon > \upsilon_b$) which are given in Table 3.

The axial displacement profile for the stress-free boundary condition is compared with finite element results in Fig. 8. Once again, excellent agreement between the simple theory and the FEM is observed.

Comparison with Finite Element Simulations

Figure 9 compares the axial strain predicted by the simplified model with the results of finite element simulations over a wide range of load speeds. The conditions other than load speed are those listed in Table 1. As this figure shows, the simplified model captures the spatially-averaged axial strains quite well. The strains in this plot are normalized by the mean hoop strain $\bar{\varepsilon}_\theta = P_o a C_t/Eh$, which is the same for all load speeds. This scaling demonstrates the substantial amplification that occurs as the bar velocity υ_b is approached.

It is interesting to note that the simplified model, despite being an unsteady model, predicts peak strains that do not vary with time. In contrast, the finite element model predicts peak axial strains that grow with time at a rate very close to $t^{2/3}$ (which is in good agreement with the theoretical predictions of [9]). The simplified model does not capture this temporal growth since this effect involves the coupling between radial, rotary, and axial modes of motion which are neglected in the simple theory.

To enable a more quantitative comparison between the predictions of the simplified model and the finite element simulations, the simulated strain traces were averaged on the intervals $[0, \upsilon t]$ and $[\upsilon t, \upsilon_b t]$ corresponding to the primary and precursor waves. These average strains are compared with the predictions of the simple model in Fig. 10. In both the precursor wave and the primary wave, the axial strain predictions of the simplified model are in very good agreement with the finite element simulations. Only near the resonant point $\upsilon/\upsilon_b = 1$ are significant differences observed. One reason for these differences is the fact that the peak strain predicted by the finite element model grows with time. The peak strain observed in the simulations is therefore limited by the finite length of the pipe, and closer agreement with the simplified model would probably be obtained if a longer pipe were simulated.

Conclusions

A simplified model was proposed for predicting the axial displacement, stress, and strain in pipes subjected to internal shock waves. This model was derived using both physical arguments from mass and momentum conservation as well as direct solution of the governing partial differential equation of motion. Comparisons with finite element simulations show that this model adequately captures the low-frequency behavior over a wide range of load speeds, with speeds varying from zero to greater than the bar speed $\upsilon_b = \sqrt{E/\rho}$. When the load speed υ approaches the bar speed, the simple model predicts a time-independent resonance with unbounded stresses and strains. In contrast, the finite element model predicts peak strains that grow with $t^{2/3}$. However, for load speeds differing by more than about 10% from υ_b, the predictions of the simple model are quite adequate.

References

[1] Beltman, W., Burscu, E., Shepherd, J., and Zuhal, L., 1999. "The structural response of cylindrical shells to internal shock loading". *Journal of Pressure Vessel Technology,* **121**(3), pp. 315–322.

[2] Beltman, W., and Shepherd, J., 2002. "Linear elastic response of tubes to internal detonation loading". *Journal of Sound and Vibration,* **252**(4), pp. 617–655.

[3] Shepherd, J. E., and Akbar, R., 2009. Forces due to detonation propagation in a bend. Tech. Rep. FM2008-002, Graduate Aeronautical Laboratories California Institute of Technology, February.

[4] Shepherd, J. E., and Akbar, R., 2009. Piping system response to detonations. results of ES1, TS1 and SS1 testing. Tech. Rep. FM2009-001, Graduate Aeronautical Laboratories California Institute of Technology, April. Revised June 2010.

[5] Karnesky, J., Damazo, J. S., Chow-Yee, K., Rusinek, A., and Shepherd, J. E., 2013. "Plastic deformation due to reflected detonation". *International Journal of Solids and Structures,* **50**(1), pp. 97–110.

[6] Timoshenko, S. P., 1934. *Theory of Elasticity*, first ed. McGraw-Hill.

[7] Kolsky, H., 1963. *Stress Waves in Solids*. Dover.

[8] Haberman, R., 2004. *Applied Partial Differential Equations*, fourth ed. Pearson Education, Inc.

[9] Schiffner, K., and Steele, C. R., 1971. "Cylindrical shell with an axisymmetric moving load". *AIAA Journal,* **9**(1), pp. 37–47.

Nomenclature

a Mean radius of pipe $0.5(R_i + R_o)$

C_t Correction factor $(R_i/a)^2$ due to thick-wall effects

E Elastic modulus of pipe

g Green's function for the wave equation

h Pipe wall thickness

N_x Axial stress resultant

N_θ Hoop stress resultant

P Pressure of shock wave

R_i Inner radius of pipe

R_o Outer radius of pipe

u Axial displacement of pipe

u_p Maximum axial displacement along pipe

w Radial displacement of pipe

V Axial velocity of pipe material $\partial u/\partial t$

ε_x Axial membrane strain

ε_θ Hoop strain

Θ Heaviside step function

ν Poisson's Ratio

ρ Pipe density

υ Speed of shock wave

υ_b Bar wave speed $\sqrt{E/\rho}$

υ_d Dilatational shell wave speed $\sqrt{E/\rho(1-\nu^2)}$

List of Tables

List of Figures

Table 1. Dimensions, material properties, and load conditions of Schedule 40 stainless steel pipe

Density ρ	kg/m^3	8040
Young's Modulus E	GPa	193
Poisson's Ratio ν	-	0.3
Bar Wave Speed υ_b	m/s	4900
Shell Dilatational Wave Speed υ_d	m/s	5190
Pressure Wave Speed υ	m/s	2088
Pressure Load P	MPa	2.52
Pipe Inner Radius R_i	mm	26.25
Pipe Wall Thickness R_o	mm	3.91
Mean radius a	mm	28.2

Table 2. Comparison of model results with the LS-Dyna solution.

Property	LS-Dyna	Model
$\dot{u}_p$ (m/s)	-0.0350	-0.0359
$\varepsilon_{x,1}$ (μstrain)	12.7	12.8
$\varepsilon_{x,2}$ (μstrain)	-16.8	-17.2
$\varepsilon_{\theta,1}$ (μstrain)	-3.92	-3.83
$\varepsilon_{\theta,2}$ (μstrain)	85	79.5

Table 3. List of expressions for the axial displacement for several different boundary conditions and load conditions. The displacement is zero if $x/t > \max(\upsilon, \upsilon_b)$.

Load Case	Boundary Condition	Displacement
$\upsilon \le \upsilon_b$	$u(0) = 0$	$u(x,t) = C_t \frac{\nu P a}{E h} \begin{cases} -\frac{\upsilon_b x}{\upsilon + \upsilon_b} & x < \upsilon t \\ \frac{\upsilon \upsilon_b}{\upsilon_b^2 - \upsilon^2}(x - \upsilon_b t) & x > \upsilon t \end{cases}$
$\upsilon \ge \upsilon_b$	$u(0) = 0$	$u(x,t) = C_t \frac{\nu P a}{E h} \begin{cases} -\frac{\upsilon_b x}{\upsilon + \upsilon_b} & x < \upsilon_b t \\ \frac{\upsilon_b^2}{\upsilon^2 - \upsilon_b^2}(x - \upsilon t) & x > \upsilon_b t \end{cases}$
$\upsilon \le \upsilon_b$	$N_x(0) = 0$	$u(x,t) = C_t \frac{\nu P a}{E h} \begin{cases} -x + \frac{\upsilon \upsilon_b}{\upsilon + \upsilon_b} t & x < \upsilon t \\ \frac{\upsilon^2}{\upsilon_b - \upsilon^2}(x - \upsilon_b t) & x > \upsilon t \end{cases}$
$\upsilon \ge \upsilon_b$	$N_x(0) = 0$	$u(x,t) = C_t \frac{\nu P a}{E h} \begin{cases} -x + \frac{\upsilon^2 t}{\upsilon + \upsilon_b} & x < \upsilon_b t \\ \left(\frac{\upsilon \upsilon_b}{\upsilon^2 - \upsilon_b^2} - 1\right)(x - \upsilon t) & x > \upsilon_b t \end{cases}$

Fig1a.tiff

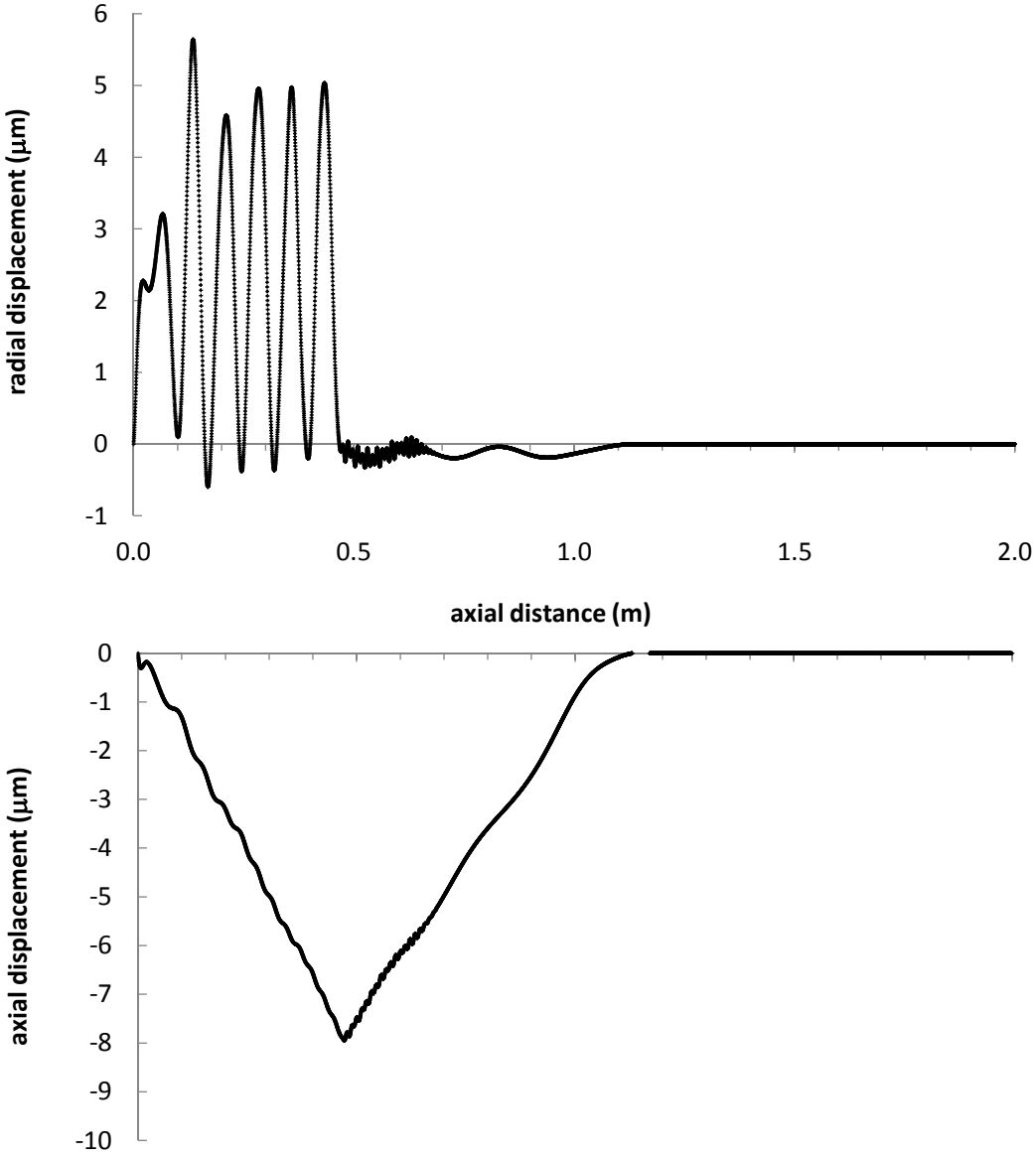

Fig. 1. Simulation results for radial and axial displacement on the outer surface of the pipe at 225 μs; the shock wave front is located at 0.47 m and the bar wave front is at 1.1 m.

Fig1b.tiff

Fig2a.tiff

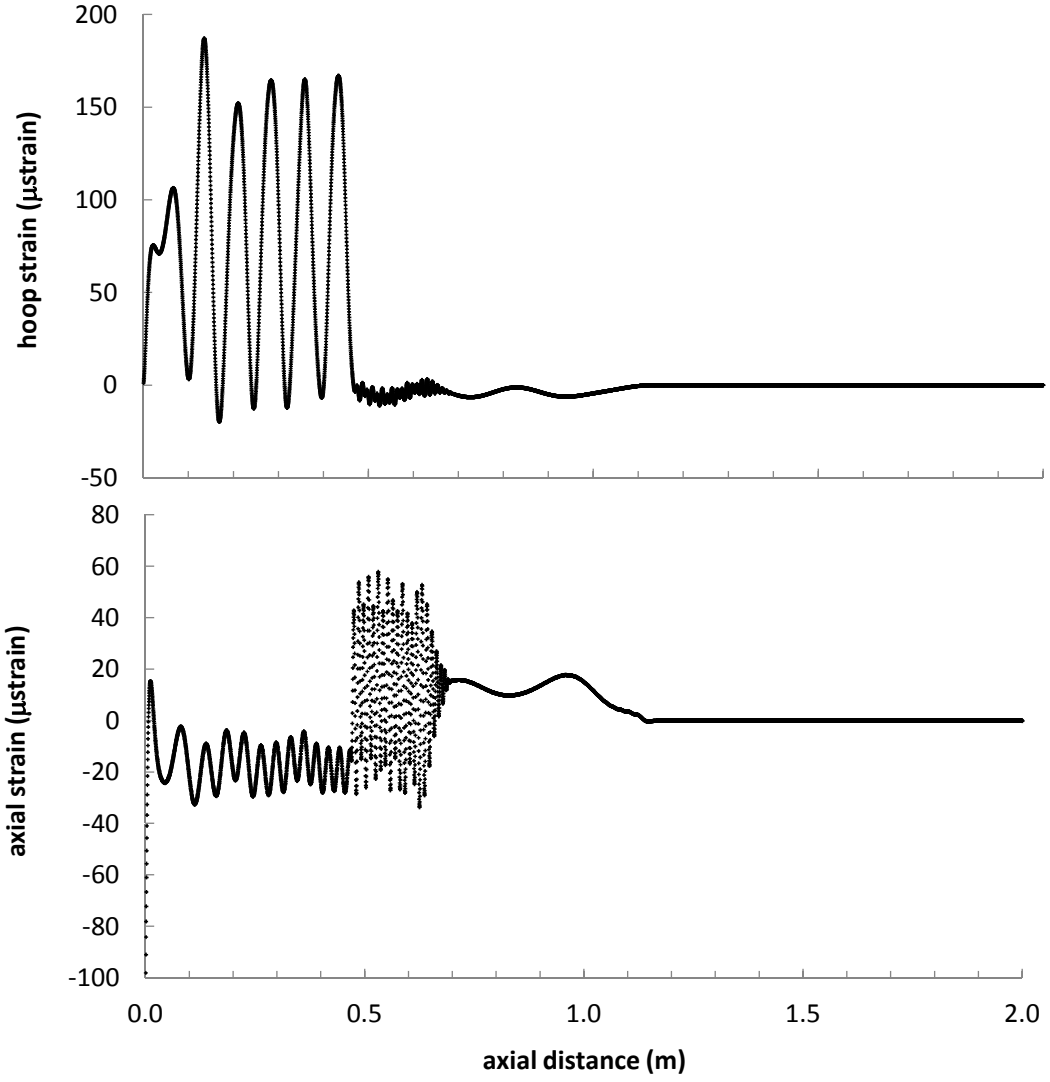

Fig. 2. Simulation results for hoop and axial strains on the outer surface of the pipe at 225 μs;

Fig2b.tiff

Fig3a.tiff

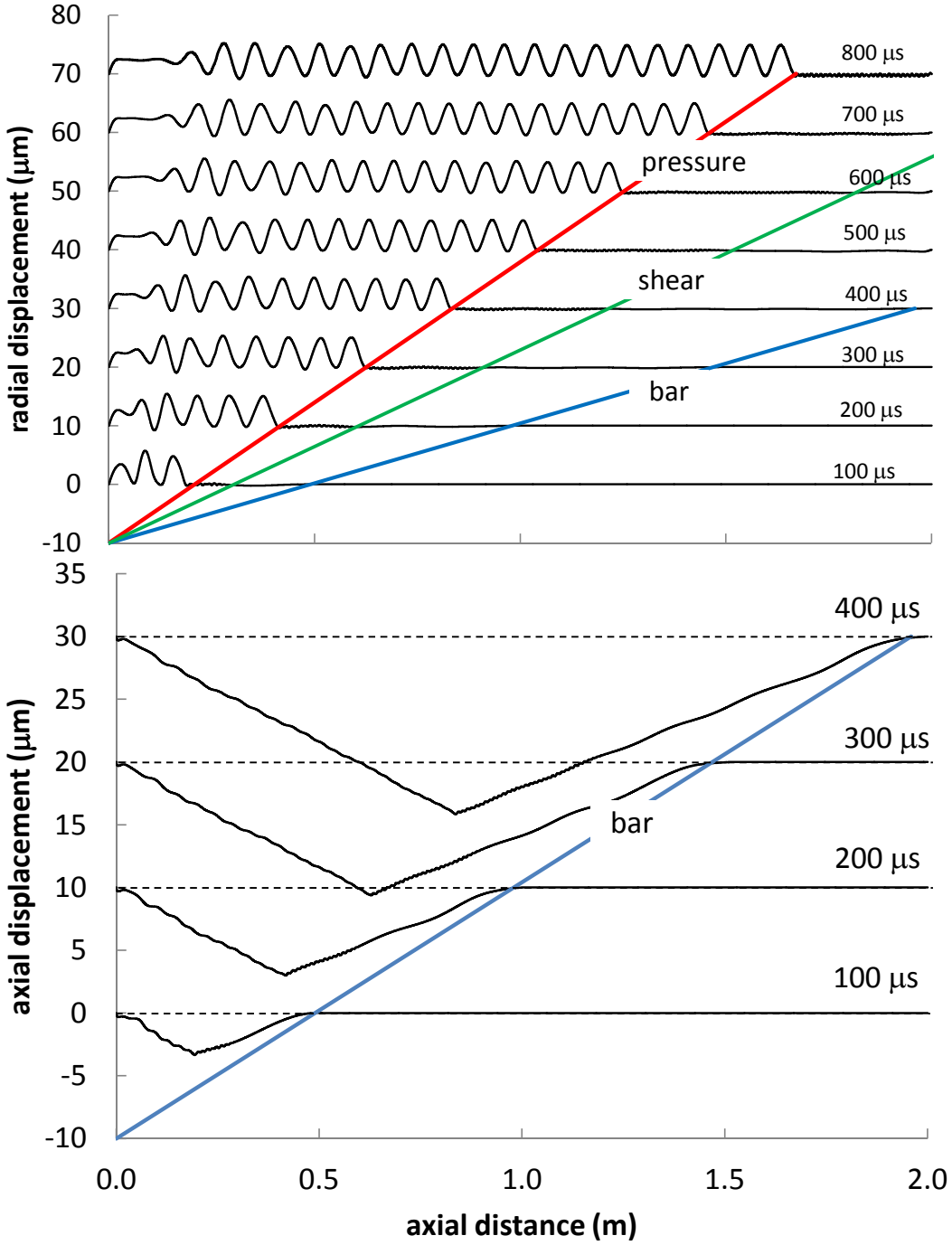

Fig. 3. Simulation results for radial and axial displacement wave systems shown at increments of 100 μs. For clarity, successive traces have the zero values offset by an amount proportional to the time increment.

Fig3b.tiff

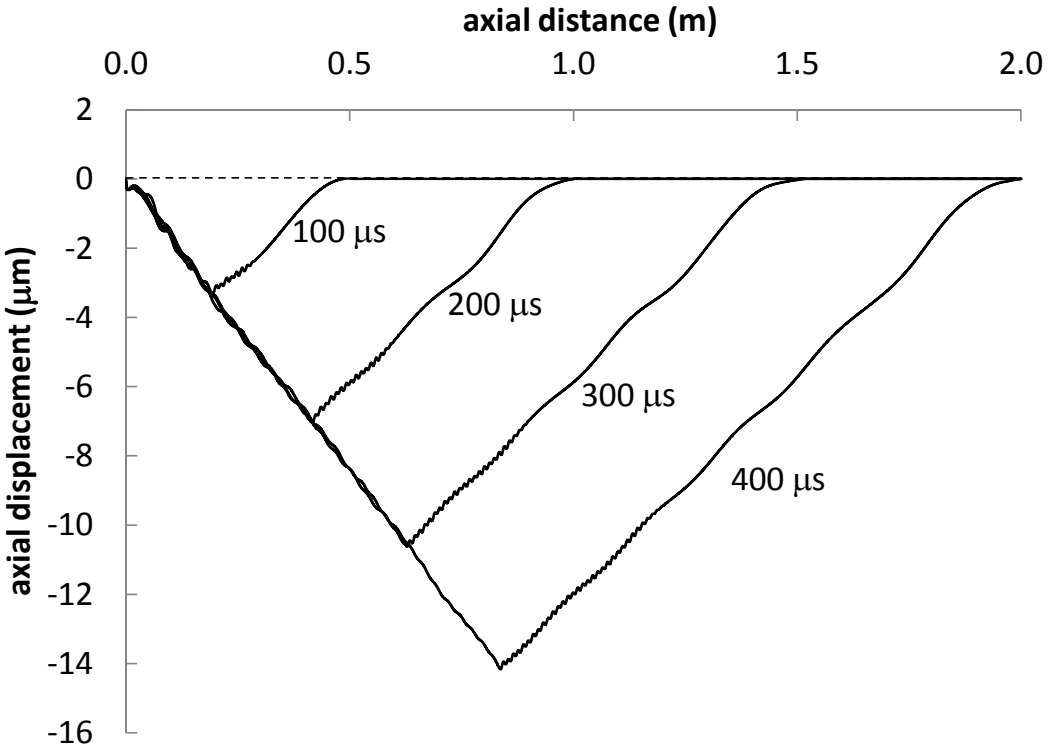

Fig. 4. Selected axial displacements from Fig. 3 shown without offsetting the zero strain.

Fig4.tiff

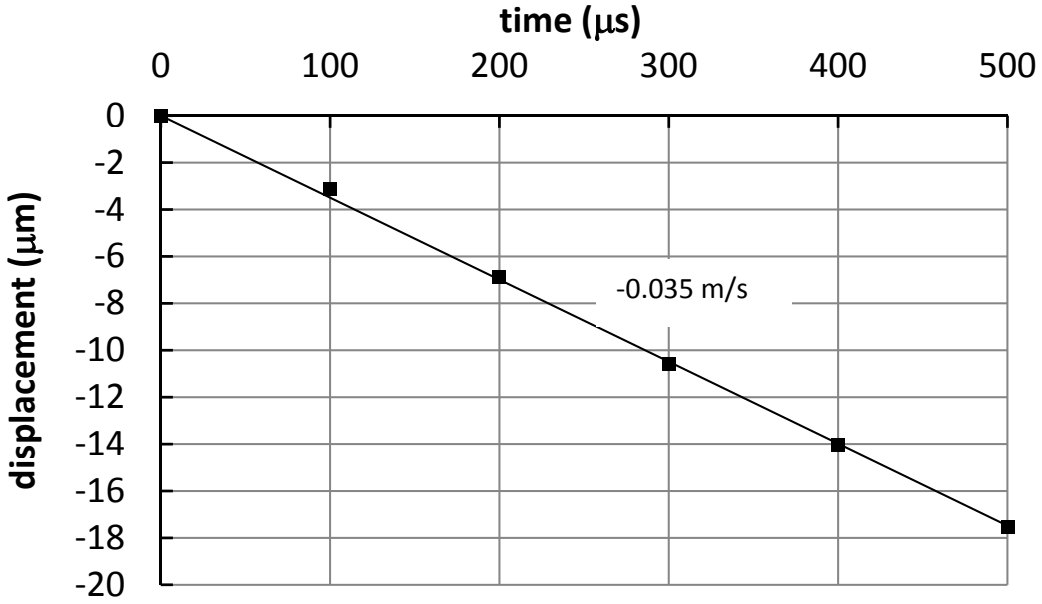

Fig. 5. Extremum axial displacement (at $x = \upsilon t$) as a function of time showing the linear relationship.

Fig5.tiff

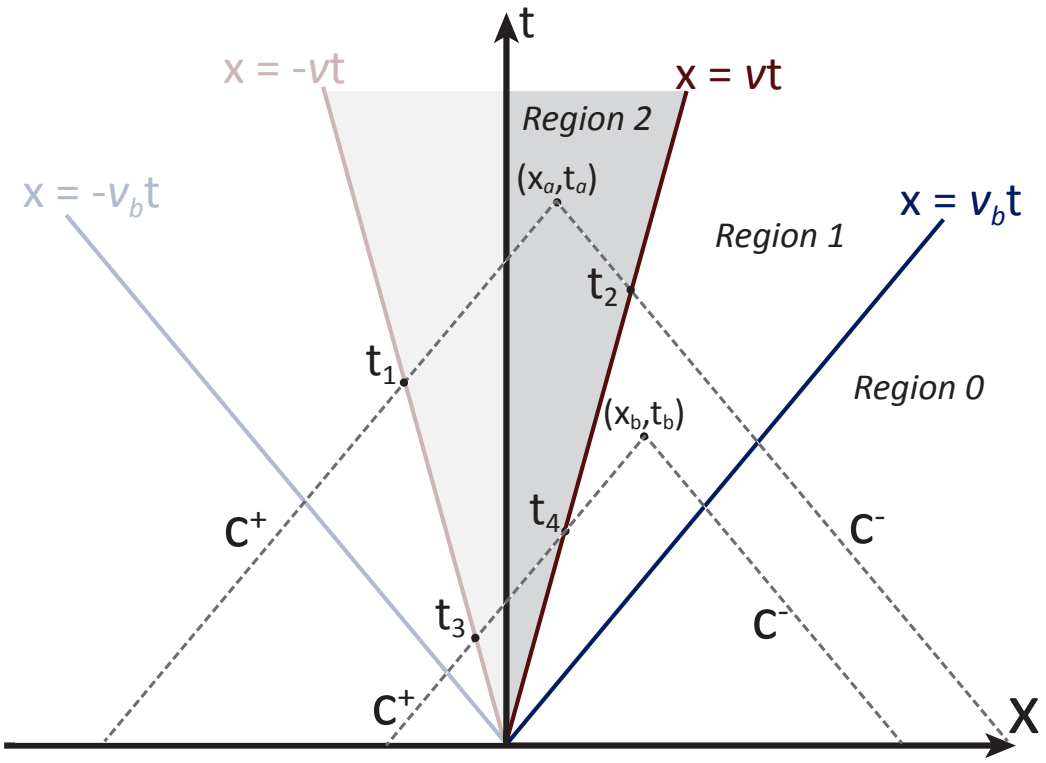

Fig. 6. Wave diagram for a shock wave traveling along a tube at speed υ.

Fig6.tiff

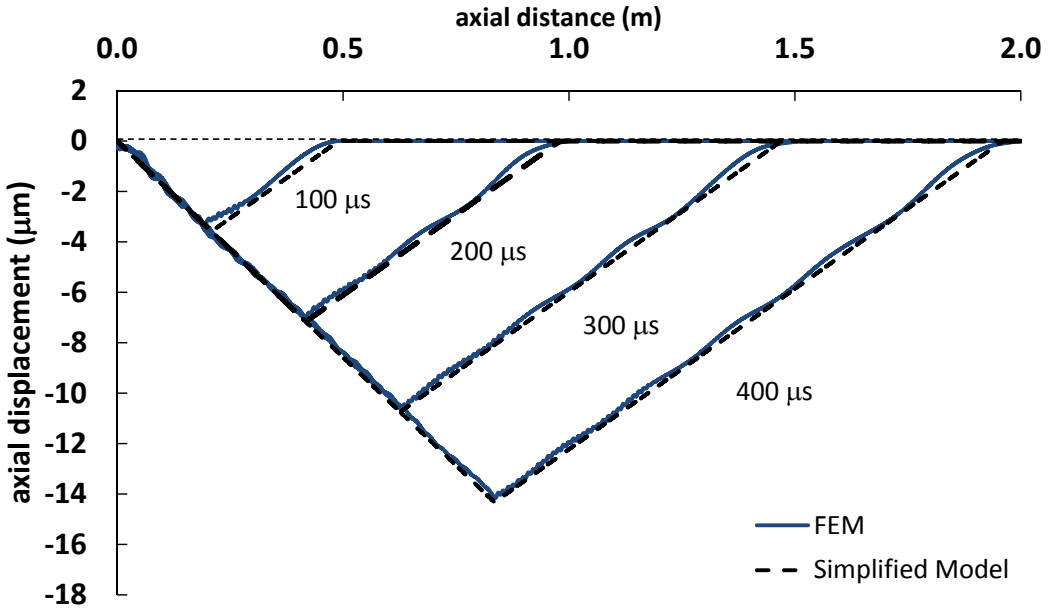

Fig. 7. Comparison of axial displacements from finite element simulations and the present simple model. Boundary condition is $u(0,t)=0$. Simulation conditions are those summarized in Table 1.

Fig7.tiff

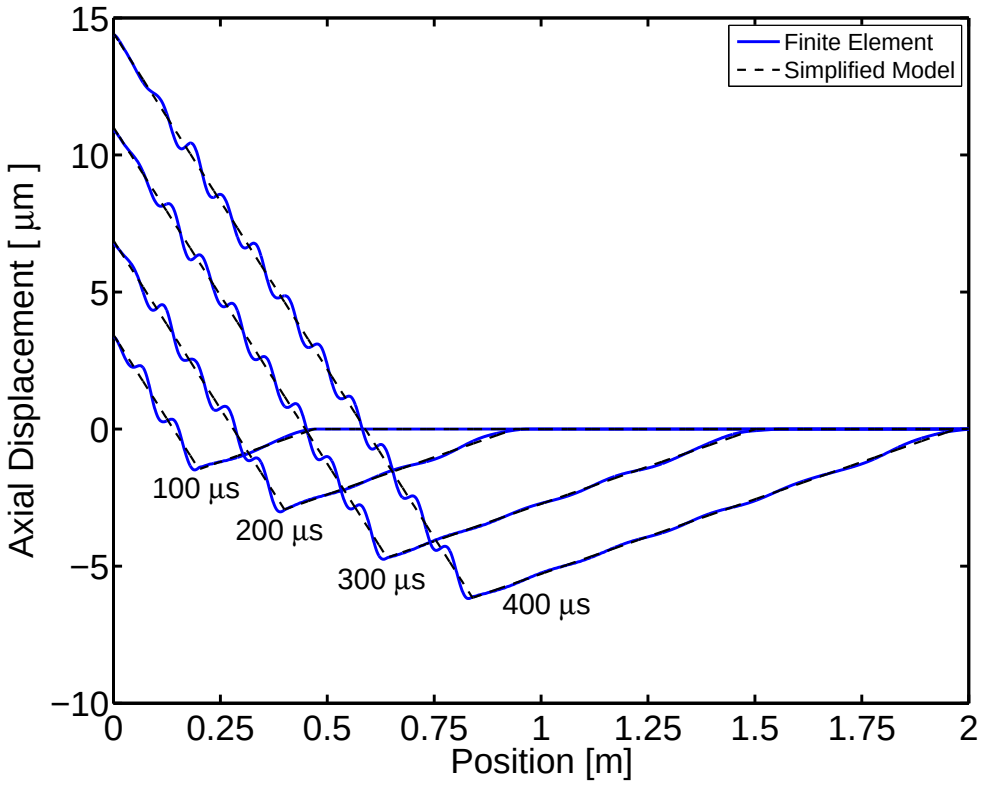

Fig. 8. Comparison of axial displacement from finite element simulations and the present simple model. Boundary condition is $N_x(0,t) = 0$. Simulation conditions are summarized in Table 1.

Fig8.tiff

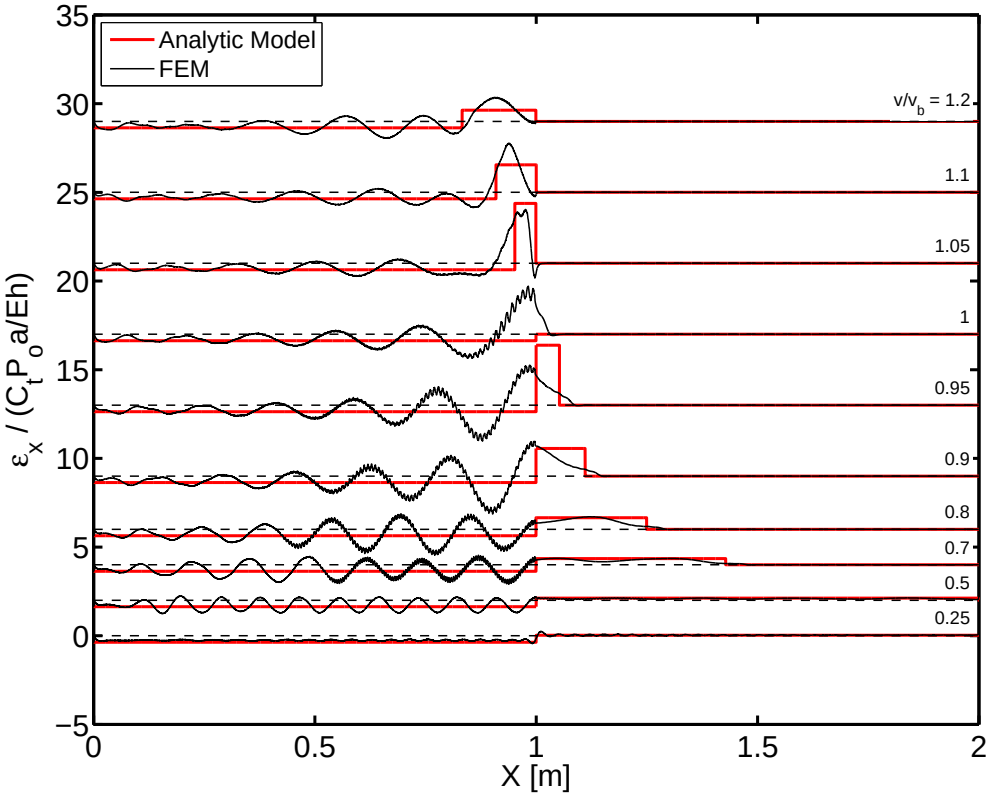

Fig. 9. Comparison of axial strain profiles for several speeds of pressure load. For the case of $\upsilon/\upsilon_b = 1.0$, the model predicts a function of infinite height and zero width. The boundary condition is $N_x(0,t) = 0$, and strains are normalized by the static hoop strain $P_o a/Eh$.

Fig9.tiff

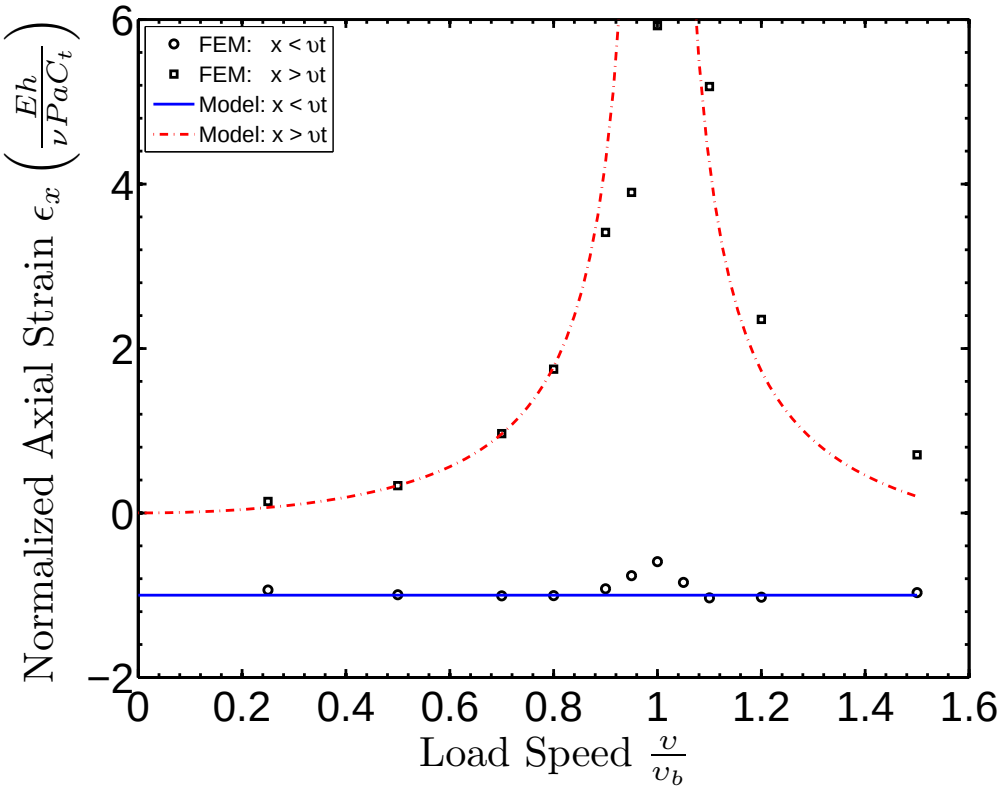

Fig. 10. Average axial strains in precursor and primary wave regions. Symbols correspond to finite element simulations and solid lines to the simple model. Boundary condition is $N_x(0,t) = 0$.

Fig10.tiff